Journal of Power Sources 467 (2020) 228350

Contents lists available at ScienceDirect

Journal of Power Sources

journal homepage: www.elsevier.com/locate/jpowsour

Effect of reacting gas flowrates and hydration on the carbonation of anion exchange membrane fuel cells in the presence of CO_2

Yiwei Zheng [a], Garrett Huang [b], Lianqin Wang [c], John R. Varcoe [c], Paul A. Kohl [b], W. E. Mustain [a,*]

[a] Department of Chemical Engineering, Swearingen Engineering Center, University of South Carolina, Columbia, SC, 29208, USA
[b] School of Chemical and Biomolecular Engineering, Georgia Institute of Technology, Atlanta, GA, USA
[c] Department of Chemistry, The University of Surrey, Guildford, Surrey, GU2 7XH, United Kingdom

HIGHLIGHTS

- AEMFCs are studied in the presence of carbon dioxide in the cathode.
- CO_2-related thermodynamic, kinetic and Ohmic voltage losses are quantified.
- The effect of operating variables on the CO_2-related voltage losses is studied.
- Conditions are shown that significantly reduce voltage loss vs. existing literature.
- High-performing AEMFCs, even with CO_2 in the cathode, are reported.

GRAPHICAL ABSTRACT

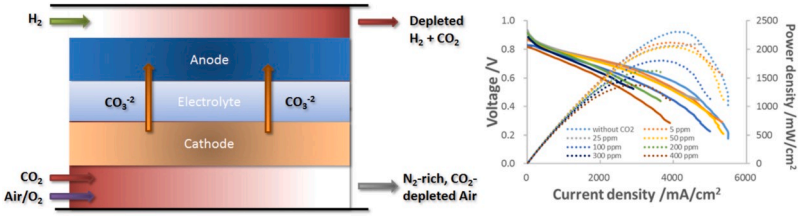

ARTICLE INFO

Keywords:
Anion exchange membrane
Fuel cell
CO_2
Carbonate
Air

ABSTRACT

Anion exchange membrane fuel cells (AEMFCs) have been widely touted as a low-cost alternative to existing proton exchange membrane fuel cells. However, one of the limitations of this technology has been the severe performance penalty related to the introduction of CO_2 to the cell – typically in the air cathode feed. Introduction of CO_2 into AEMFCs results in cell carbonation, which imparts thermodynamic, kinetic and Ohmic overpotentials that can add up to hundreds of millivolts. Therefore, it is important to find strategies and operational protocols for AEMFCs that minimize these overpotentials. In this paper, we investigate the impacts of the anode and cathode flowrate, as well as the cell hydration level, on the extent of cell carbonation and cell polarization. Key findings include: (1) decreasing the cathode flowrate generally decreases the total CO_2-related voltage loss while changing the anode flowrate has a minimal effect; (2) increasing cell hydration helps to mitigate the performance loss in the presence of CO_2; and (3) operational combinations are found that significantly reduce the CO_2 penalty compared to the present literature.

1. Introduction

Alkaline-based fuel cells can have advantages over their more popular counterpart, the proton exchange membrane fuel cell (PEMFC). For instance, traditional alkaline fuel cells (AFCs) can be operated with much lower quantities of noble metal catalyst or even with non-noble metal electrocatalysts like nickel, silver, etc. [1] Also, the electrolyte, liquid KOH, is much less expensive than Nafion®. For this reason, AFCs are still being pursued by companies such as AFC Energy PLC in the UK.

However, despite their possible cost advantages, AFCs are not being widely implemented today and the primary reason is that the OH^- anions in the electrolyte react with CO_2 in the ambient air cathode feed to

* Corresponding author.
E-mail address: mustainw@mailbox.sc.edu (W.E. Mustain).

https://doi.org/10.1016/j.jpowsour.2020.228350
Received 12 March 2020; Received in revised form 7 May 2020; Accepted 12 May 2020
Available online 26 May 2020

form (bi)carbonates [2–4] (Equations (1) and (2)).

$$OH^- + CO_2 \leftrightarrow HCO_3^- \quad (1)$$

$$HCO_3^- + OH^- \leftrightarrow CO_3^{2-} + H_2O \quad (2)$$

The resulting CO_3^{2-} anions react with the mobile K^+ ions in the electrolyte to form the low solubility compound K_2CO_3, which can precipitate onto the cathode electrode, lowering AFC performance and stability. Strategies have been proposed to solve this CO_2 poisoning problem. For example, Cifrain and Kordesch [5] found that the negative effects of CO_2 poisoning can be partly mitigated by circulating the electrolyte. Another possibility is to change the electrolyte from a liquid (aqueous salt solution) to an ion conducting polymer, i.e. by the use of an anion exchange membrane (AEM) – creating so-called anion exchange membrane fuel cells (AEMFCs). AEMFCs avoid salting because the positively charged cations are stationary (typically covalently bound to the polymer backbone) and not alkaline earth ions, eliminating the possibility for precipitates to form. As a result, the CO_3^{2-} anions are able to be transported through the AEM, and they are able to carry a portion of the charge from the cathode to the anode to complete the electrochemical circuit [6,7]. However, this does not mean that carbonation has a null effect on AEMFC behavior.

For many years it was very difficult to understand the effects of carbonation on AEMFC behavior due to the chemical instability of available AEMs and very low cell performance. Fortunately, the past few years have seen a significant improvement in both AEM properties and AEMFC performance. For instance, there have been several reports of AEMs with hydroxide conductivity of over 100 mS/cm (60 °C–80 °C) [8–10] and recent reports of AEMs having conductivity over 200 mS/cm (at 80 °C) [11]. State-of-the-art AEMFCs have the ability to achieve peak power densities over 3 W cm^{-2} operating on H_2/O_2 gas feeds [8]. One notable example by Huang et al. reported AEMs made from poly(norbornene) block copolymer with very high hydroxide conductivity, 198 mS/cm, and record peak power density in a hydrogen/oxygen fuel cell, 3.4 W/cm^2 at 80 °C [11]. Also, the performance stability of AEMFCs has improved dramatically during this time, with multiple groups reporting 500+ hour stability at low degradation rates (5–10%) [12–15].

Now that AEMFC performance and stability have been enhanced to the point where their future deployment in real applications is realistic, it is an important time in AEMFC development to begin to answer some of the contemporary issues that have to date been mostly put aside in the literature, including operating on real air, which contains CO_2, leading to the carbonation discussed above. Recently, there have been several experimental [16–21] and modeling [22–25] studies that have allowed researchers in the field to well-understand how adding CO_2 to high performing AEMFCs influences their behavior.

There are three primary mechanisms for voltage loss. First, as carbonate anions are formed at the AEMFC cathode from Equations (1) and (2), they migrate through the AEM from the air cathode to the hydrogen anode. Carbonate mobility is lower than hydroxide mobility, which leads to an increase in the area-specific resistance (ΔASR). Second, because hydrogen does not react with the carbonate directly at relevant potentials, carbonates are not immediately released on arrival to the anode as CO_2. Instead, there is a time lag while the carbonates accumulate at the anode and the pH of that electrode drops [26] – forcing the reverse of Equations (1) and (2) to occur before the CO_2 is eventually released. The drop in the anode pH leads to a thermodynamically-driven increase in the anode potential (ΔV_{Nernst}), reducing the overall cell voltage. This has been successfully modeled by Gerhardt et al. [23], Krewer et al. [24] and Wrubel et al. [27]. Third, the accumulation of carbonates in the anode causes low local OH^- concentrations throughout the anode, leading to an increase in the anode charge transfer resistance, (ΔR_{ctHOR}). This third effect was captured quite well in the Gerhardt model [23]. Therefore, the operating voltage for an AEMFC with CO_2 in the cathode feed can be described by Equation (3)[16]:

$$V_{cell} = V_{OCV} - i(R_{\Omega,OH} + R_{ctORR} + R_{mtORR} + R_{ctHOR}) - \Delta V_{Nernst} - i(\Delta ASR + \Delta R_{ctHOR}) \quad (3)$$

In total, the voltage loss from these three mechanisms are typically several hundred millivolts under operating conditions of practical interest. The Nernstian voltage loss (ΔV_{Nernst}) and increase in the charge transfer resistance ($i\Delta R_{ctHOR}$) dominate the CO_2-related performance loss whereas the voltage loss related to the ASR ($i\Delta ASR$) increase is often a minor contributor (<10% of the total loss) [16,23].

There are several pathways by which the CO_2-related voltage losses can mitigated. In our previous work [16], it was shown that increasing the AEMFC operating current density and increasing the cell temperature can slightly mitigate the negative effects of CO_2. Lowering the CO_2 concentration in the reacting gas below 400 ppm can also help, but at high cathode flowrates, even having 5 ppm CO_2 in the cathode feed has been untenably harmful, resulting in CO_2-related voltage losses of about 100 mV [16,23,28]. Therefore, it is important to continue to explore the impact of cell operating conditions on the tolerance of AEMFCs to the presence of CO_2 in the cathode feed. In this study, three new variables are investigated: the anode flowrate, the cathode flowrate, and the cell hydration. The cathode reacting gas flowrate is expected to be important because it sets the total dose of CO_2 that is fed to the cell. The anode flowrate can influence the degree of cell carbonation because it will inevitably control the concentration of CO_2 (i.e. via dilution) in the anode stream. The CO_2 in the hydrogen stream, which is usually recirculated, can be taken back up into the cell. Lastly, the level of cell hydration may influence how much CO_2 can be taken up by the cell (i.e. Equations (1) and (2)) as well as its overall concentration.

2. Experimental

2.1. Electrode preparation

The electrodes in this work were prepared using a method that has been detailed in our previous publications [10,15,29,30]. Briefly, the anode and cathode catalysts were 60 wt% PtRu supported on Vulcan XC-72R (Alfa Aesar HiSPEC 10000, 2:1 ratio of Pt:Ru by mass – Pt nominally 40 wt%, and Ru, nominally 20 wt%) and 40 wt% Pt supported on Vulcan XC-72R (Alfa Aesar HiSPEC 4000, Pt nominally 40 wt%), respectively. Electrode preparation was initiated by placing an ethylene tetrafluoroethylene (ETFE) benzyltrimethylammonium (BTMA) solid powder anion exchange ionomer (AEI, ion-exchange capacity IEC = 1.24 mmol g^{-1}) into a mortar and grinding it by hand with a pestle for 10 min. The catalyst powder, Vulcan carbon (XC-72R, Cabot), and 1 mL of Millipore deionized (DI, 18.2 MΩ cm resistivity) water were added to the mortar and ground for an additional 10 min. The mass fraction of AEI in the catalyst layer was always 0.20 and the mass fraction of carbon was maintained at 0.48 for both electrodes. Next, the catalyst-AEI slurry was transferred to a centrifuge tube. Solvent was added and the mixture was sonicated (Fisher Scientific FS30H) for 60 min. The water in the ultrasonic bath was maintained below 5 °C to avoid degrading the supported catalyst and the AEI, and to maximize the electrochemically active area. The ink dispersions were sprayed onto Toray TGP-H-060 gas diffusion layers with 5 wt% PTFE wetproofing with an Iwata Eclipse HP-CS (the carrier gas was 15 psig ultra high purity, UHP, N_2) to create gas diffusion electrodes (GDEs). The target catalyst loading on both the anode and cathode GDEs was 0.6 ± 0.1 mg_{Pt} cm^{-2}.

2.2. Anion exchange membrane fuel cell (AEMFC) assembly and break-in procedure

Before cell assembly, the GDEs were soaked in 1 M aqueous KOH solutions (made from Fisher Chemical pellets/certified ACS and DI water) for 60 min, exchanging the solution twice during this time. At the same time, the AEM was soaked in an identical solution. After the 1 h

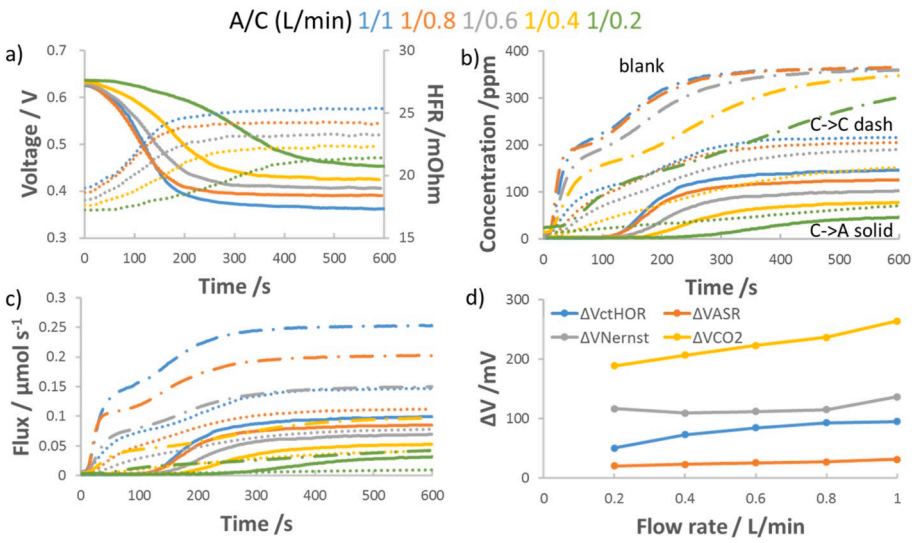

Fig. 1. Effect of cathode flowrate on the carbonation of an AEMFC operating at 1 A/cm^2 and 60 °C with a LDPE-BTMA AEM, 400 ppm CO_2 fed to cathode at t = 0 s, 1 L/min anode flowrate, and 5 cm^2 active area. a) Voltage loss (solid lines) and HFR increase (dotted lines) following the introduction of CO_2 into the cathode; b) Concentration of CO_2 in the anode (solid lines) and cathode (dotted lines) effluent streams; c) CO_2 flux in the anode and cathode effluent; d) deconvoluted CO_2-related voltage losses. In panels a)-c), the results are color-coded based on flowrate, as indicated at the top of the figure. In panels b) and c), the cathode "blank" plots are shown by combination dash-dot lines. (For interpretation of the references to color in this figure legend, the reader is referred to the Web version of this article.)

soak, excess KOH was removed from the GDEs and AEMs before cell assembly. The GDEs and AEMs were pressed together in the cell to form each membrane electrode assembly (MEA) in situ with no prior hot pressing. The MEAs were loaded into 5 cm^2 Scribner hardware between two single pass serpentine flow graphite plates. The MEA was sealed and compressed with 6 mil (152 μm) PTFE gaskets with 20%–25% pinch at 5.1 N m torque. An 850e Scribner Fuel Cell Test Station was used to control the gas stream dew points, cell temperature, gas flowrates and the operating current density.

Four different AEMS were used in this study. The first was a benzyltrimethyl ammonium-(BTMA)-type radiation-grafted AEM [31] made from a 25 μm low density polyethylene (LDPE) precursor film (LDPE-BTMA, IEC = 2.5 mmol g^{-1}), which was used when investigating the influence of flowrate on the CO_2-related voltage losses. The second was an ETFE-BTMA-based radiation-grafted AEM [32] (ETFE-BTMA, IEC = 2.1 mmol g^{-1}, 50 μm when fully swollen in water), which was used when probing the effect of hydration on CO_2 uptake at 60 °C. Third, a tetra-block poly(norbornene) (PNB) copolymer with 64 mol% halogenated monomer with different mole percent of cross-linking agent *N,N,N′,N′*-tetramethyl-1,6-hexanediamine (TMHDA) were used. The mole percent of TMHDA relative to the number of head-groups was 5 mol%, 15 mol% and 25 mol%. These films are denoted as GT-64-X, where X is the crosslinker content. For example, GT-64-5 has 5 mol% TMHDA with respect to the moles of head-group within the copolymer. GT-64-X AEMs were tested to show how AEM water uptake can be tuned to influence cell carbonation. Lastly, a BTMA-functionalized radiation-grafted AEM made from 15 μm high density polyethylene (HDPE-BTMA, IEC = 2.4 mmol g^{-1}) [33] was used for experiments that were trying to find the minimum CO_2-related voltage loss within the operating conditions of this study. The choice of using multiple AEMs was purposeful. First, it shows how widespread the carbonation issue is. Voltage loss upon exposure to CO_2 is not a chemistry-specific phenomenon; it is intrinsic to operation of AEMFCs. Second, there are some physical properties of the various AEMs that are useful to show. For example, some AEMs have poorer stability at high temperature or lower water uptake – though developing an understanding of the explicit effects of membrane physical properties is not attempted here. To be consistent, each experimental set in this work is internally consistent, deploying a single AEM.

Before CO_2 measurements were made, all cells underwent a break-in procedure. First, the cell was brought to its operating temperature under N_2 flow on both sides of the cell at 100% relative humidity (RH). Then, the feed gases were switched to UHP H_2 and O_2 (Airgas) at the anode and cathode, respectively. Next, the cell was operated potentiostatically, stepwise from 0.7 V to 0.3 V (0.1 V steps, held for a minimum of 30 min at each step) as the reacting gas dew points were optimized per our standard procedure [15,29,30]. The optimized reacting gas dew points were very repeatable from cell-to-cell; dew points were typically 50 °C at the anode and 52 °C at the cathode for an AEMFC operating at 60 °C. Following the optimization of the reacting gas dew points, the cell was operated galvanostatically at 1.0 A cm^{-2} and allowed to equilibrate for at least 30 min before CO_2 exposure was initiated. Multiple cells were constructed and tested for each measurement.

2.3. AEMFC carbon dioxide measurements

Following the break-in procedure and 30 min equilibration, the cell current was held constant and 400 ppm CO_2 was added to the UHP O_2 cathode stream. CO_2 was added to O_2 in lieu of air in order to simplify observations, because air has an additional O_2 mass transport impact (e.g. N_2 dilution) during cell operation that is largely eliminated by utilizing O_2 as the reacting gas. The flowrates for O_2 and H_2 were varied from 0.2 to 1 L min^{-1}. Typically, after CO_2 addition, the cell was operated for 10 min, which was much longer than the time required to reach quasi-steady-state operation (typically < 5 min, though lower CO_2 concentrations took longer to reach steady-state). After 30 min operation at constant current, CO_2 was removed from the gas stream and the cell was allowed to decarbonate for an initial 10 min. After this, the cell was fully decarbonated by lowering the cell potential to 0.1 V for 2 min, after which no CO_2 emission was measured in the anode stream and the operating voltage returned to the value observed before CO_2 was added. The concentration of CO_2 emitted from the anode and cathode was constantly monitored in real time using a PP Systems WMA-5 non-dispersive infrared CO_2 gas analyzer (a water trap was placed in-line before the WMA-5 in order to preserve the unit and its calibration).

Table 1
Degree of steady-state carbonation as function of cathode flowrate feeding with 400 ppm CO_2.

Anode/Cathode Flowrate (L/min)	1/1	1/0.8	1/0.6	1/0.4	1/0.2
AEMFC carbonate N_{CO2}/μmol	21 ± 3	17 ± 2	13 ± 2	8 ± 2	4 ± 2
Anode carbonate/μmol	8 ± 2	7 ± 2	7 ± 2	8 ± 2	8 ± 2

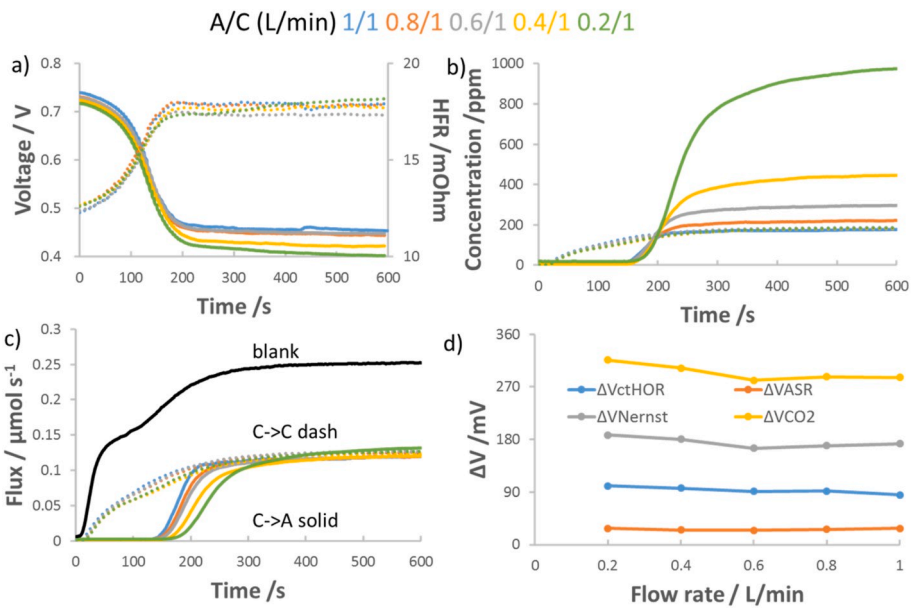

Fig. 2. Anode flowrate effect on AEMFC carbonation and performance loss. AEMFC operating at 1 A/cm^2 and 60 °C with a LDPE-BTMA AEM, 400 ppm CO_2 fed to cathode at t = 0 s, 1 L/min anode flowrate, and 5 cm^2 active area. a) Voltage loss (solid lines) and HFR increase (dotted lines) following the introduction of CO_2 into the cathode; b) Concentration of CO_2 in the anode (solid lines) and cathode (dotted lines) effluent streams; c) CO_2 flux leaving the anode and cathode; and d) deconvoluted CO_2-related voltage losses.

3. Results and discussion

3.1. Influence of flowrate on AEMFC performance with 400 ppm cathode CO_2

The effect of cathode flowrate (oxygen with 400 ppm CO_2) on the behavior of a carbonated AEMFC is presented in Fig. 1. As shown in Fig. 1a, the CO_2-related voltage loss decreased (i.e. improved) approximately linearly with decreasing cathode gas flowrate, showing that the total dose of CO_2 fed to the cell plays an important role in carbonation. Additionally, as shown in Table 1, the steady-state carbonation of the AEM and electrode ionomer in the operating cell increased with higher oxidant flowrate. As described in our previous publication [16], the carbonate content in the AEMFC can be estimated by first converting the CO_2 concentration vs. time data (Fig. 1b) from the anode and cathode exhaust into flux vs. time data (Fig. 1c) and then integrating the area under the flux curves for the anode exhaust, cathode exhaust and a "blank". The blank is a direct measure of the amount of CO_2 added to the cathode, a measurement that is made in the absence of the anionic polymer. For more information on the "blank" experiment, please see the Supporting Information file. Hence, the amount of carbonate/CO_2 in the cell for any operating condition can be calculated (N_{CO2}) by Equation (4):

$$N_{CO2} = \int \text{"blank"}(t)\,dt - \int \text{"anode exhaust"}(t)\,dt - \int \text{"cathode exhaust"}(t)\,dt \quad (4)$$

Evidence for the uptake of CO_2 into the cell is also given by the cell's high frequency resistance (HFR with ASR ≅ HFR × A where A = geometric cell area), shown in Fig. 1a. Lower cathode flowrates resulted in a lower HFR. It was also interesting to note that it took a longer time for the cell to reach a stable HFR value and voltage at a lower flowrate. These dynamics also match well with what was observed with the CO_2 concentration in the anode exhaust, Fig. 1b. Even at the same operating current density (same charge flux through the AEM), the CO_2 breakthrough time in the anode exhaust was longer at lower flowrates. This shows that CO_2 accumulation is slower in the AEMFC anode at lower flowrate, that is, the flux of carbonate across the cell is lower. The data also shows that the flux of CO_2 leaving the anode (Fig. 1c, calculations in the Supporting Information) at steady state is lower at lower flowrate; hence, the rate of CO_2 uptake at the cathode is also less at lower flowrate.

It might be thought that combining the lower rate of anode carbonate accumulation combined with a lower incoming flux would reduce the amount of carbonate in the anode during cell operation. However, the release of CO_2 requires the accumulation of carbonates in the anode. Eventually the number of supplied carbonate ions result in a sufficiently high carbonate concentration at the anode such that the reverse of Equations (1) and (2) occurs. The speciation shifts from CO_3^{2-} to HCO_3^- and then finally CO_2. Because CO_2 release is always observed at the anode, it is possible that the anode carbonate concentration may not be significantly different across the range of flowrates. To estimate the total amount of carbonate in the anode electrode, the CO_2 was removed from the cathode feed until the cell reached a new steady state. The resulting cell was then pulsed to 0.1 V and the amount of CO_2 in the anode exhaust was measured versus time. The integral of the CO_2 concentration vs. time can be used as an estimate total amount of carbonate left in the cell, which, after the new steady state, should overwhelmingly be in the anode [16]. These values are also reported in Table 1 where it was found that the total amount of anode carbonate was nearly unchanged with cathode flowrate. This effect of AEMFC N_{CO2} vs. total amount of anode carbonate also has implications on the individual contributions to the CO_2-related voltage loss, discussed above. However, before deconvoluting the effect of the cathode flowrate on the root causes for cell voltage loss, it is important to point out from Fig. 1b that AEM-like devices can also act as CO_2-separators which can simultaneously generate energy, unlike traditional approaches which consume energy.

Though Fig. 1a is informative, data following the release of CO_2 is needed in order to deconvolute the CO_2-related voltage loss into its fundamental constituents: ΔASR, ΔV_{Nernst} and ΔR_{ctHOR}. That raw data is shown in Figure S2 – S6 in the Supporting Information and the quantified values for ΔASR, ΔV_{Nernst} and ΔR_{ctHOR} are presented in Table S1. The details for performing the deconvolution was extensively described and demonstrated elsewhere [16], but a short description and visualized calculation of the decoupling process is provided in the Supporting Information file. Fig. 1d graphically display the results of the deconvolution. In Fig. 1d, the ΔASR increased almost linearly with the cathode flowrate, and the total amount of carbonate in the cell shown in Table 1. ΔR_{ctHOR} increased with flowrate as the amount of carbonate in the cell increased, with the smallest increase at the lowest flowrates. Fig. 1d presents ΔV_{Nernst} as a function of cathode flowrate as well as the voltage loss caused by the other two mechanisms, allowing ΔV_{Nernst}, ΔV_{ASR} ($\Delta V_{ASR} = i\Delta ASR$) and ΔV_{ctHOR} ($\Delta V_{ctHOR} = i\Delta R_{ctHOR}$) to be compared.

Table 2
Degree of steady-state carbonation as function of anode flowrate feeding with 400 ppm CO_2.

Anode/Cathode Flowrate (L/min)	1/1	0.8/1	0.6/1	0.4/1	0.2/1
AEMFC carbonate/μmol	19 ± 2	20 ± 2	20 ± 2	27 ± 3	24 ± 4
Anode carbonate/μmol	11 ± 2	11 ± 6	14 ± 4	14 ± 2	18 ± 2

Here, the overall voltage loss was dominated by the Nernstian loss and the increase in the charge transfer resistance. It should be noted that the Nernstian loss was the most significant, and was nearly constant regardless of the flowrate, which agrees well with the anode carbonation state in Table 1. This suggests that the outermost part of the anode, where the potential is measured experimentally, likely remains firmly dominated by the bicarbonate/CO_2 equilibrium at all flowrates. The next largest contributor to the cell performance loss was the charge transfer resistance. It was also the most affected by flowrate. For completeness, Figure S7 and Table S2 show the cathode flowrate effect with a GT-64-15 AEM as well, which showed the same behavior.

Next, the effect of lowering the anode reacting gas flowrate was investigated and the results are shown in Fig. 2. In general, the anode flowrate did not have a significant impact on the CO_2-related overpotential. Fig. 2a shows that the CO_2 overpotential only very slightly increased with decreasing H_2 flowrate. This was not due to a significant increase in the amount of carbonate in the system, as evidenced by the similar HFR for all cases and the total cell carbonation being similar (Table 2). This suggests that the main reason for increased polarization is increased carbonate concentration in the anode, particularly right at the anode/GDL interface, which is evidenced by larger Nernstian and charge transfer losses at lower flowrates as well as the semi-quantitative measurement of anode CO_2 content (using the procedure described above for the cathode) as summarized in Table 2.

It was observed that as the anode flowrate was decreased, the CO_2 concentration in the anode exhaust increased, which is shown in Fig. 2b. In fact, it was possible for the concentration of CO_2 in the anode exhaust to be significantly higher than the CO_2 concentration in the cathode feed, showing that these devices can act as CO_2 concentrators. It was also observed that the cathode exhaust nearly always contained 200 ppm CO_2 regardless of the H_2 flowrate, showing that the extent of carbonation near the cathode was very low, and suggesting that the cathode likely sees minimal resistance to CO_2 uptake and carbonate formation. The carbonate uptake and flux across the cell was essentially independent of anode flowrate (Fig. 2c) because of the rapid reaction between carbon dioxide and hydroxide. Finally, as described above, the polarization losses were deconvoluted from the data where CO_2 was supplied and removed from the cathode (Figure S8 - S12 in the Supporting information file). As shown in Fig. 2d, none of the three major contributors to the CO_2-related overpotential changed significantly as the anode flowrate was changed.

The final flowrate-related experiment involved lowering the flowrates of both the anode and cathode gases simultaneously and equally. As shown in Fig. 3a, the voltage and HFR showed similar behavior to Fig. 1a as CO_2 is applied. It is noted that the initial operating voltage is different in each case due to performance differences at lower reacting gas flowrates; low flowrates can make it more difficult to manage the AEMFC water production at the anode and this has an effect on the cell performance [15,29]. In fact, in these cells, stable operation at 0.2 L/s was not possible and is, thus, not reported here. There were some notable CO_2-related cell dynamics at this condition that were not obvious by looking at the data in Figs. 1 and 2. For instance, in Fig. 3b, the amount of CO_2 in the exhausts were comparable, suggesting a balance between the dosing and removal. In addition, Fig. 3c shows higher flux at reasonably higher flowrates. But the most surprising observations were made after deconvoluting the data sets where CO_2 was first applied and then released (shown in Figure S13 - S15 in the Supporting Information) to determine the contribution of each of the fundamental causes of CO_2-related voltage loss. The Nernstian, Ohmic and kinetic losses from the addition of CO_2 at various identical anode/cathode flowrates are summarized in Fig. 3d. Despite the dynamics in the CO_2 flux (Fig. 3c) at various flowrates, lowering the flowrates symmetrically did not significantly impact the total CO_2-derived overpotentials nor did it drastically change any individual contributor, though there does seem to be some interplay between ΔR_{ctHOR} and ΔV_{Nernst} where the former slightly increases with flowrate and the latter decreases. This can be understood based on the dynamics of the system where despite the fact that lower cathode flowrates reduce the dosing of the cell, the lower

Table 3
Degree of steady-state carbonation as function of anode/cathode flowrate feeding with 400 ppm CO_2.

Anode/Cathode Flowrate (L/min)	0.8/0.8	0.6/0.6	0.4/0.4
AEMFC carbonate/μmol	15 ± 4	14 ± 4	15 ± 3
Anode carbonate/μmol	8 ± 3	9 ± 2	11 ± 2

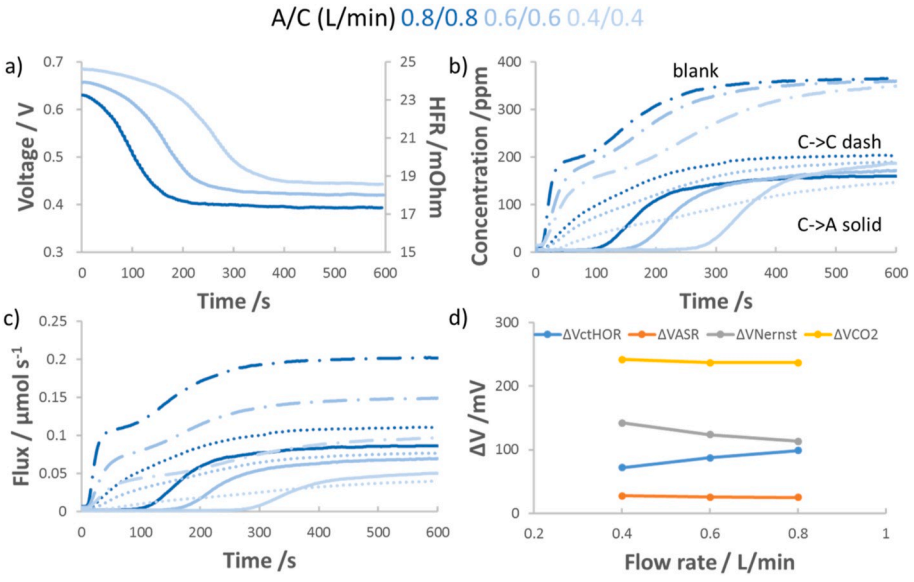

Fig. 3. Effect of symmetrically reducing the anode and cathode flowrate on AEMFC carbonation. All cells were operated at 1 A/cm^2 and 60 °C with 25 μm LDPE-BTMA AEM, and 5 cm^2 active area. The concentration of CO_2 fed to the cathode was 400 ppm, applied at t = 0 s. a) voltage losses and HFR increases after the introduction of CO_2, b) CO_2 emission from the anode (solid lines) and cathode (dotted lines); c) CO_2 flux; and d) deconvoluted CO_2 related voltage losses at the investigated symmetrical flowrates.

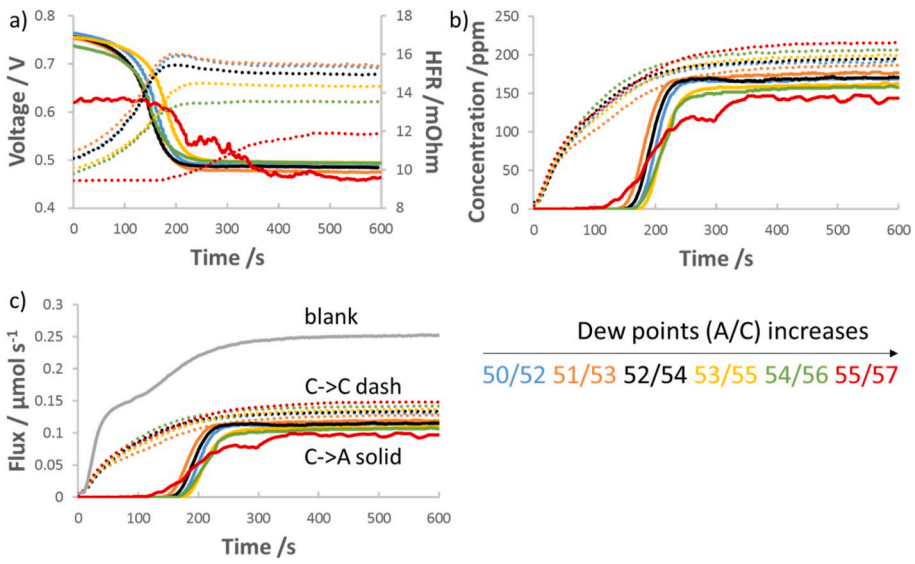

Fig. 4. Effect of water content on the carbonation of AEMFCs operating at 1 A/cm^2 and 60 °C with ETFE-BTMA AEM, 5 cm^2 active area. 400 ppm CO_2 in O_2 was fed to cathode at t = 0 s, and UHP H_2 to the anode, both at a rate of 1 L/min a) voltage loss and HFR increase as function of dew points (anode/cathode); b) CO_2 emission from the anode (solid lines) and cathode (dotted lines); c) CO_2 flux.

Table 4
Influence of hydration on the CO_2-related overpotential and degree of carbonation for an AEMFC operating at 60 °C.

Anode/Cathode Dew Points	50/52	51/53	52/54	53/55	54/56	55/57
CO_2 overpotential/V	0.277	0.277	0.272	0.261	0.244	0.151
△HFR/mOhm	4.73	4.43	4.37	4.21	3.72	2.66
AEMFC carbonate/ µmol	17 ± 1	16 ± 1	14 ± 1	18 ± 1	15 ± 1	17 ± 1
Anode carbonate/ µmol	16 ± 1	15 ± 1	17 ± 1	17 ± 1	17 ± 1	12 ± 1

anode flowrate makes it more difficult to remove carbonate from the system. Thus, at lower flowrates, as summarized in Table 3, despite similar overall amounts of carbonate in the system, the anode itself appears to have a higher total amount of CO_2 at lower flowrate than at higher flowrate, which is expected to increase the charge transfer resistance. The Nernstian voltage loss did slightly increase with decreasing flowrates, which is most likely the result of carbonate accumulation in regions of the cell other than the anode. This causes the pH difference between the anode and cathode to be less at lower flowrates than higher flowrates. Figure S16 and Table S2 show the same flowrate effect with a different membrane, GT-64-15, which again showed the same behavior.

3.2. Effect of hydration on the performance of AEMFCs operating with 400 ppm CO_2

Another variable that may influence the CO_2 uptake in the AEM cell is cell hydration. There are multiple ways to manipulate the amount of water in the cell. One way is to change the dew point of the anode and cathode reacting gases. The results of doing so on the CO_2-related voltage loss is shown in Fig. 4a and summarized in Table 4. At low-to-intermediate dew point values, the total CO_2-related overpotential very slightly decreased with increased hydration (evidenced the by the lower HFR in Table 4). As the dew points were increased, the concentration and flux of CO_2 in the anode exhaust decreased while the concentration leaving the cathode increased, shown in Fig. 4b–c. This appears to confirm that increasing the amount of free water in the cell slightly lowers CO_2 uptake in the cathode. The presence of this free water most likely leads to a dilution effect, where the environment is made less basic in nature, decreasing the CO_2 solubility. At the highest dew point settings, the total CO_2 overpotential was low, but this was subject to a tradeoff where the high hydration levels led to anode flooding (excess liquid water), which reduced overall cell performance and resulted in fluctuations in the cell voltage (cathode/anode dew points = 55/57 °C in Fig. 4a).

A second pathway to change the water content of the cell is to manipulate the polymer itself. One way to do that is to vary the amount of water that can be taken up by the polymer, which can be done by changing its degree of crosslinking or the ratio of the monomers in the copolymer. To show this effect, the percentage of crosslinker in a GT-64

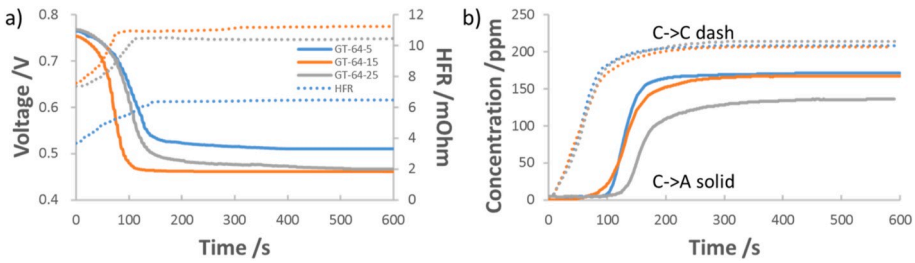

Fig. 5. Influence of water uptake on AEMFC carbonation for cells operated at 1 A/cm^2 and 74/74/80 °C (A/C/cell) with 10 µm thick GT-64-X AEMs. The GT-64-X AEMs contain increasing crosslinker content (5%, 15%, and 25%, denoted as X = 5, 15, 25, respectively). 400 ppm CO_2 was fed to cathode, 5 cm^2 active area. Specifically shown are a) voltage loss and HFR increase and b) CO_2 emission from the anode (solid lines) and cathode (dotted lines) as crosslinker content is increases.

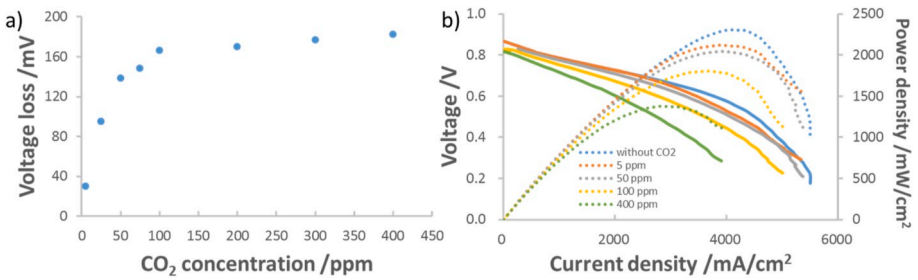

Fig. 6. a) Voltage loss as function of CO_2 concentration at 2 A/cm^2 cell discharge; b) Power density curves for AEMFCs operated at various CO_2 concentrations in O_2, up to 400 ppm. The cell was operated at 80 °C with anode/cathode dew points of 78/80 °C. The anode flowrate was 1 L/min and the cathode flowrate was 0.2 L/min. The membrane was HDPE-BTMA (ca. 30 μm thick when fully hydrated). 5 cm^2 active area.

polynorbornene copolymer AEM was varied from 5% to 25%. As the degree of crosslinking is increased, the water uptake is reduced [10]. Therefore, in this study, the GT-64-5 AEM had the highest water content and GT-64-25 had the lowest water content. As shown in Fig. 5a, the overall voltage loss decreased with increasing water content. GT-64-5, GT-64-15, and GT-64-25 AEMFCs showed overall CO_2-related the voltage losses of 254 mV, 292 mV, and 300 mV, respectively. Figs. 4 and 5 confirm that increasing the water content in an operating AEMFC helps reduce the CO_2-related performance penalty. Fig. 5b reports the CO_2 concentrations in the anode and cathode effluents for the GT-64 AEMs with varied crosslinking. Interestingly, the overall amount of CO_2 taken up by the cell does not appear to be significantly changed by the crosslinker content. But, the lower crosslinker content (higher water content) did have a clear effect on the HFR and voltage loss. This suggests that the membrane water can influence the cell behavior even if the total CO_2 content of the cell is similar.

3.3. *Optimizing operating conditions to minimize the effect of CO_2 on AEMFCs*

The results above show that lower cathode flowrate (i.e. high ratio between the anode/cathode flowrate) and higher cell water content both contribute to lower total CO_2-related voltage loss. The experimental results in this work also agree with the modeling work by Gerhardt et al. [23] and Setzler et al. [26] who both showed that the degree of carbonation increased with decreased cathode flowrate. In addition to these two mechanisms, our previous work [16] showed that higher operating current density, lower the CO_2 concentration, and higher temperature also lowered CO_2-related voltage losses. Therefore, we deployed a combination of the above advantageous conditions and operated a cell at 80 °C, anode/cathode dew points of 78/80 °C, high anode flowrate at 1 L/min and low cathode flowrate at 0.2 L/min. We then recorded point-by-point data with varied CO_2 content in the cathode at a constant current density of 2 A/cm^2 (Fig. 6a). Polarization curves were also recorded at several cathode CO_2 concentrations (Fig. 6b).

As shown in Fig. 6a, under these "optimized" conditions, operating an AEMFC with low CO_2 concentrations did not lead to catastrophic voltage losses. In fact, only a 30 mV voltage loss was observed with 5 ppm CO_2 in the cathode feed. When 400 ppm CO_2 oxygen was fed to the cathode, the total CO_2-related voltage loss was 182 mV, which is half of the previously reported value [16], showing that the operating conditions are vitally important in dictating CO_2 tolerance. As the CO_2 concentration exceeded 100 ppm, there was an asymptotic behavior where increasing from 100 ppm to 400 ppm did not significantly affect the CO_2-related voltage losses. However, increasing the concentration of CO_2 in the cathode feed led to further decreases in the achievable mass transport limiting current and peak power density. However, most AEMFCs (like most PEMFCs) would not actually be operated near the peak power density. Considering a more realistic operating point (2 A/cm^2 at 0.6 V) for various applications, including automotive, there was only *ca.* 20% reduction in the power density with 400 ppm CO_2 in the cathode gas compared to benchmark CO_2-free conditions. Some slightly lower concentrations (<100 ppm) experience less than a 10% loss. This seems to provide some good news – that AEMFCs can be operated with CO_2 in the cathode stream, even at 400 ppm, without catastrophic performance losses. It is important to acknowledge that pure oxygen instead of air is being used here when the latter has reduced overall performance. The focus here is on the intrinsic effect of CO_2, justifying the use of O_2, but it is noted that the use of air is a more realistic operating condition for automotive and other applications.

4. Conclusions

In this study, it experimentally shown in high performance AEMFCs that decreasing the total CO_2 dose to the cell (by decreasing the cathode flowrate) and increasing the level of hydration in an operating AEMFC are two possible pathways to lowering the CO_2-related voltage losses. Considering the fundamental mechanisms for CO_2-related voltage losses, the Nernstian voltage loss was the dominant loss and it was not affected by the gas flowrates. The next most important contributor to voltage loss was the anode charge transfer resistance, which increased with increasing O_2 flowrate and decreasing H_2 flowrate. The Ohmic resistance increased with increasing cathode flowrate, but was a minor overall contributor to overall cell performance loss. Lastly, a new set of operting conditions, which lowered the total CO_2-related overpotentials to achieve practical current-voltage values was found and demonstrated. These insights will help both modeling groups and experimental researchers to better understand the operation of AEMFCs with CO_2 containing cathode feeds, as well as allow them to pose and assess new solutions.

It is also shown that AEM-like devices may be able to act as CO_2 separators that can simultaneously generate power. Finally, as the anode feed flowrate decreased, the CO_2 concentration in the anode increased to levels several times larger than the cathode inlet concentration, showing that these devices can act as energy-generating CO_2 concentrators.

Declaration of competing interest

The authors declare that they have no known competing financial interests or personal relationships that could have appeared to influence the work reported in this paper.

CRediT authorship contribution statement

Yiwei Zheng: Investigation, Formal analysis, Data curation, Writing - review & editing. **Garrett Huang:** Investigation, Formal analysis. **John R. Varcoe:** Conceptualization, Writing - review & editing, Funding acquisition, Supervision, Project administration. **Paul A. Kohl:** Conceptualization, Writing - review & editing, Funding acquisition, Supervision, Project administration. **W.E. Mustain:** Conceptualization, Writing - review & editing, Funding acquisition, Supervision, Project

administration.

Acknowledgements

The authors gratefully acknowledge the financial support of the U.S. National Science Foundation (Award Number: 1803189) for the effort expended by Y.Z. and W.E.M at USC. G.H. and P.K. at Georgia Tech gratefully acknowledge the financial support of the ARPA-E IONICS program (United States Department of Energy, grant number DE-AR0000769). The University of Surrey effort was facilitated using resources provided by UK EPSRC grant EP/M014371/1.

Appendix A. Supplementary data

Supplementary data to this article can be found online at https://doi.org/10.1016/j.jpowsour.2020.228350.

References

[1] G. Merle, M. Wessling, K. Nijmeijer, J. Membr. Sci. 377 (2011) 1–35.
[2] E. Gülzow, M. Schulze, J. Power Sources 127 (2004) 243–251.
[3] A. Sen, A. Tewari, V. Sambhy, M. Urquidi Macdonald, J. Power Sources 153 (2006) 1–10.
[4] L.A. Adams, S.D. Poynton, C. Tamain, R.C.T. Slade, J.R. Varcoe, ChemSusChem 1 (2008) 79–81.
[5] K.V. Kordesch, M. Cifrain, J. Power Sources 127 (2004) 234–242.
[6] J.A. Vega, C. Chartier, W.E. Mustain, J. Power Sources 195 (2010) 7176–7180.
[7] K.N. Grew, W.K.S. Chiu, J. Electrochem. Soc. 157 (2010) B327.
[8] P.A. Kohl, G. Huang, M. Mandal, Electrochem. Soc. Meet. Abstr. 33 (2019), 1733–1733.
[9] L. Wang, J.J. Brink, J.R. Varcoe, Chem. Commun. 53 (2017) 11771–11773.
[10] G. Huang, M. Mandal, X. Peng, A.C. Yang-Neyerlin, B.S. Pivovar, W.E. Mustain, P. A. Kohl, J. Electrochem. Soc. 166 (2019) F637–F644.
[11] M. Mandal, G. Huang, N.U. Hassan, X. Peng, T. Gu, A.H. Brooks-starks, B. Bahar, W.E. Mustain, P.A. Kohl, J. Electrochem. Soc. 167 (2020), 054501.
[12] S.M. Alia, K. Neyerlin, K. Hurst, J.W. Zack, S.A. Mauger, W.W. McNeary, A. Weimer, W. Medlin, S. Zaccarine, C. Ngo, S. Pylypenko, K. Buechler, B. S. Pivovar, Electrochem. Soc. Meet. Abstr. 44 (2018), 1505–1505.
[13] S.M. Alia, S. Stariha, R.L. Borup, B.S. Pivovar, Electrochem. Soc. Meet. Abstr. 46 (2018), 1604–1604.
[14] W.E. Mustain, Electrochem. Soc. Meet. Abstr. 47 (2018), 1637–1637.
[15] T.J. Omasta, X. Peng, W.E. Mustain, Electrochem. Soc. Meet. Abstr. 30 (2018), 1754–1754.
[16] Y. Zheng, T.J. Omasta, X. Peng, L. Wang, J.R. Varcoe, S. Pivovar, W.E. Mustain, Energy Environ. Sci. 12 (2019) 2806–2819.
[17] Z. Siroma, S. Watanabe, K. Yasuda, K. Fukuta, H. Yanagi, ECS Trans. 33 (2010) 1935–1943.
[18] Y. Matsui, M. Saito, A. Tasaka, M. Inaba, ECS Trans. 25 (2010) 105–110.
[19] M. Inaba, Y. Matsui, M. Saito, A. Tasaka, K. Fukuta, S. Watanabe, H. Yanagi, Electrochemistry 5 (2011) 322–325.
[20] H. Yanagi, K. Fukuta, ECS Trans. 16 (2008) 257–262.
[21] W.A. Rigdon, T.J. Omasta, C. Lewis, M.A. Hickner, J.R. Varcoe, J.N. Renner, K. E. Ayers, W.E. Mustain, J. Electrochem. Energy Convers. Storage 14 (2017) 1–8.
[22] M.R. Gerhardt, L.M. Pant, H.-S. Shiau, A.Z. Weber, ECS Trans. 86 (2018) 15–24.
[23] M.R. Gerhardt, L.M. Pant, A.Z. Weber, J. Electrochem. Soc. 166 (2019) F3180–F3192.
[24] U. Krewer, C. Weinzierl, N. Ziv, D.R. Dekel, Electrochim. Acta 263 (2018) 433–446.
[25] J.A. Wrubel, A.A. Peracchio, B.N. Cassenti, T.D. Myles, K.N. Grew, W.K.S. Chiu, J. Electrochem. Soc. 164 (2017) F1063–F1073.
[26] B.P. Setzler, Y. Yan, Electrochem. Soc. Meet. Abstr. (2017) 1654, 01.
[27] J.A. Wrubel, A.A. Peracchio, B.N. Cassenti, K.N. Grew, W.K.S. Chiu, J. Electrochem. Soc. 166 (2019) 810–820.
[28] B.P. Setzler, L. Shi, T. Wang, Y. Yan, Electrochem. Soc. Meet. Abstr. 34 (2019) 1824.
[29] T.J. Omasta, A.M. Park, J.M. Lamanna, Y. Zhang, X. Peng, L. Wang, D.L. Jacobson, J.R. Varcoe, D.S. Hussey, B.S. Pivovar, W.E. Mustain, Energy Environ. Sci. 11 (2018) 551–558.
[30] T.J. Omasta, L. Wang, X. Peng, C.A. Lewis, J.R. Varcoe, W.E. Mustain, J. Power Sources (2017) 205–213.
[31] L. Wang, J.J. Brink, Y. Liu, A.M. Herring, J. Ponce-González, D.K. Whelligan, J. R. Varcoe, Energy Environ. Sci. 10 (2017) 2154–2167.
[32] L. Wang, E. Magliocca, E.L. Cunningham, W.E. Mustain, S.D. Poynton, R. Escudero-cid, M.M. Nasef, J. Ponce-gonzález, R. Bance-souahli, Green Chem. 19 (2017) 831–843.
[33] L. Wang, X. Peng, W.E. Mustain, J.R. Varcoe, Energy Environ. Sci. 12 (2019) 1575–1579.